Supporting Information for

Theoretically designing of polar van der Waals heterostructure for photocatalytic overall water splitting

Siwei Lin[1], Jie Shen[1], Rui Xiong[1,*], Yinggan Zhang[2,*], Libin Chen[1], Cuilian Wen[1], and Baisheng Sa[1,*]

[1]*State Key Laboratory of Green and Efficient Development of Phosphorus Resources, Materials Genome Institute, College of Materials Science and Engineering, Fuzhou University, Fuzhou 350108, P. R. China.*

[2]*College of Materials, Xiamen Key Laboratory of Electronic Ceramic Materials and Devices, Fujian Provincial Key Laboratory of Theoretical and Computational Chemistry, Xiamen University, Xiamen 361005, P. R. China*

Corresponding Author:

rxiong421@163.com (R. Xiong);

ygzhang@xmu.edu.cn (Y. Zhang);

bssa@fzu.edu.cn (B. Sa)

Table S1. The calculated lattice constant a, bond length d, and bandgaps E_g of Al_2O_3 and other monolayers.

Monolayer	a (Å)	E_g (eV)
Al_2O_3	2.951	4.13
WO_2	2.840	1.97
TiF_2	2.858	2.13
PdO_2	3.085	2.98
MoO_2	2.826	1.45
Ti_2CO_2	3.030	1.04

Table S2. The binding energy E_f and formation energy E_b for heterostructures of in different stacking configurations.

Heterostructure	Stacking	a (Å)	d (Å)	E_f (eV)	E_b (meV/Å^2)
Ti_2CO_2/Al_2O_3-P↑	I	2.980	2.665	-1.338	-27.224
	II	2.985	2.434	-1.384	-34.150
	III	2.980	3.029	-1.288	-21.098
	IV	2.983	2.452	-1.374	-33.118
	V	2.980	3.031	-1.286	-20.861
	VI	2.982	2.550	-1.354	-29.026
Ti_2CO_2/Al_2O_3-P↓	I	2.982	2.598	-1.347	-26.823
	II	2.982	2.562	-1.342	-26.417
	III	2.980	3.041	-1.276	-18.907
	IV	2.980	2.707	-1.276	-18.898
	V	2.980	3.041	-1.278	-19.117
	VI	2.984	2.528	-1.360	-28.335
MoO_2/Al_2O_3-P↑	I	2.884	2.670	-0.838	-24.785
	II	2.886	2.533	-0.854	-27.190
	III	2.882	3.070	-0.788	-18.373
	IV	2.886	2.546	-0.856	-27.340
	V	2.882	3.070	-0.788	-18.441
	VI	2.883	2.713	-0.836	-24.531
MoO_2/Al_2O_3-P↓	I	2.883	2.543	-0.840	-24.311
	II	2.882	2.587	-0.825	-22.530
	III	2.881	3.064	-0.780	-17.118
	IV	2.882	2.576	-0.828	-22.820
	V	2.881	3.064	-0.780	-17.067
	VI	2.883	2.504	-0.838	-24.115
PdO_2/Al_2O_3-P↑	I	2.996	2.301	-0.911	-37.252
	II	3.018	3.040	-0.791	-19.159
	III	3.003	3.041	-0.857	-27.015
	IV	2.986	2.527	-0.860	-27.704
	V	2.997	2.284	-0.912	-37.384
	VI	2.984	2.961	-0.786	-19.074
PdO_2/Al_2O_3-P↓	I	2.986	2.481	-0.833	-22.720
	II	2.983	2.954	-0.770	-15.620
	III	2.990	2.338	-0.860	-25.904
	IV	2.989	2.394	-0.860	-25.974
	V	2.985	2.556	-0.831	-22.464
	VI	2.983	2.954	-0.771	-15.734

Table S3. The binding energy E_f and formation energy E_b for heterostructures of in different stacking configurations.

Heterostructure	Stacking	a (Å)	d (Å)	E_f (eV)	E_b (meV/Å^2)
TiF_2/Al_2O_3-P↑	I	2.912	2.604	-0.820	-19.591
	II	2.912	2.582	-0.825	-20.334
	III	2.910	3.018	-0.780	-14.794
	IV	2.913	2.558	-0.830	-20.670
	V	2.910	3.018	-0.781	-14.866
	VI	2.911	2.614	-0.815	-18.935
TiF_2/Al_2O_3-P↓	I	2.914	2.562	-0.842	-22.562
	II	2.913	2.606	-0.829	-21.047
	III	2.911	3.023	-0.793	-16.703
	IV	2.913	2.574	-0.835	-21.830
	V	2.911	3.023	-0.792	-16.623
	VI	2.913	2.581	-0.837	-21.982
WO_2/Al_2O_3-P↑	I	2.887	2.739	-0.848	-22.707
	II	2.887	2.675	-0.859	-24.146
	III	2.886	3.061	-0.805	-17.523
	IV	2.888	2.622	-0.862	-24.441
	V	2.886	3.061	-0.805	-17.543
	VI	2.887	2.665	-0.844	-22.202
WO_2/Al_2O_3-P↓	I	2.888	2.578	-0.861	-24.266
	II	2.887	2.693	-0.846	-22.443
	III	2.886	3.063	-0.805	-17.609
	IV	2.887	2.964	-0.849	-22.869
	V	2.886	3.063	-0.805	-17.598
	VI	2.887	2.678	-0.859	-23.980

Table S4. The Bader charge data for the Ti_2CO_2/Al_2O_3-P↓ heterostructure.

Constituent Monolayer	Element	Actual Charge (e)	Total
Al_2O_3	Al 1	-2.9815	0.0037
	Al 2	-2.9843	
	O 1	1.9045	
	O 2	2.0812	
	O 3	1.9839	
Ti_2CO_2	Ti 1	-1.4888	-0.0037
	Ti 2	-1.4707	
	C 1	1.1734	
	O 1	0.8903	
	O 2	0.8903	

Table S5. The Bader charge data for the WO_2/Al_2O_3-P↓ heterostructure.

Constituent Monolayer	Element	Actual Charge (e)	Total
Al_2O_3	Al 1	-2.9802	0.0006
	Al 2	-2.9831	
	O 1	1.9012	
	O 2	2.0831	
	O 3	1.9796	
WO_2	Ti 1	-1.6025	-0.0006
	O 1	0.7981	
	O 2	0.8039	

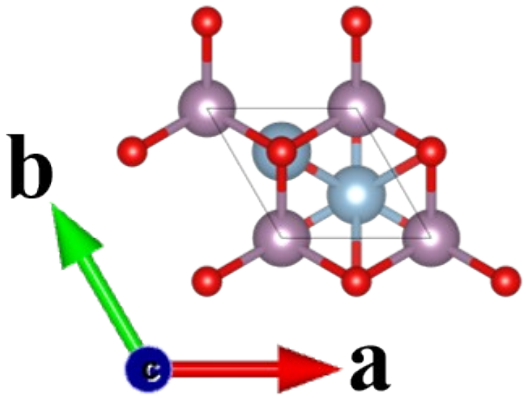

Fig. S1. Schematic of the cross-sectional area calculation.

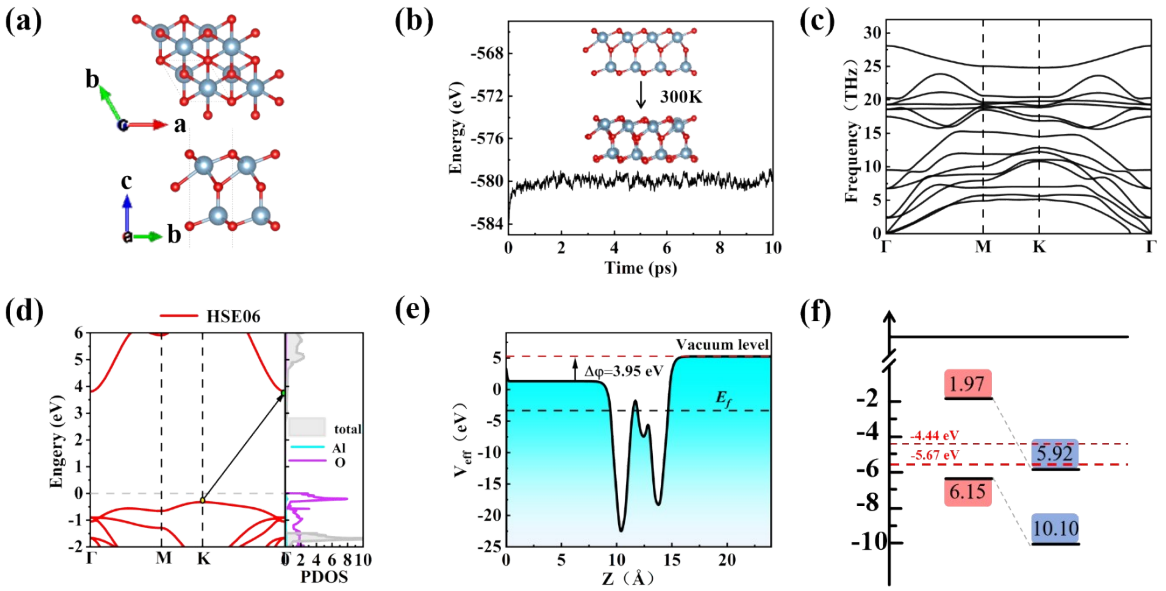

Fig. S2. (a)Top and side view of α-Al_2O_3 monolayer. (b) and (c) show the phonon spectrum and *ab initio* molecular dynamics (AIMD) simulation of the α-Al_2O_3 monolayer, respectively. Band structure of α-Al_2O_3 monolayer(d) at the HSE06 levels. (e) The planar-averaged electrostatic potential for α-Al_2O_3 along the z-axis. (f) The band edge positions of α-Al_2O_3 monolayer.

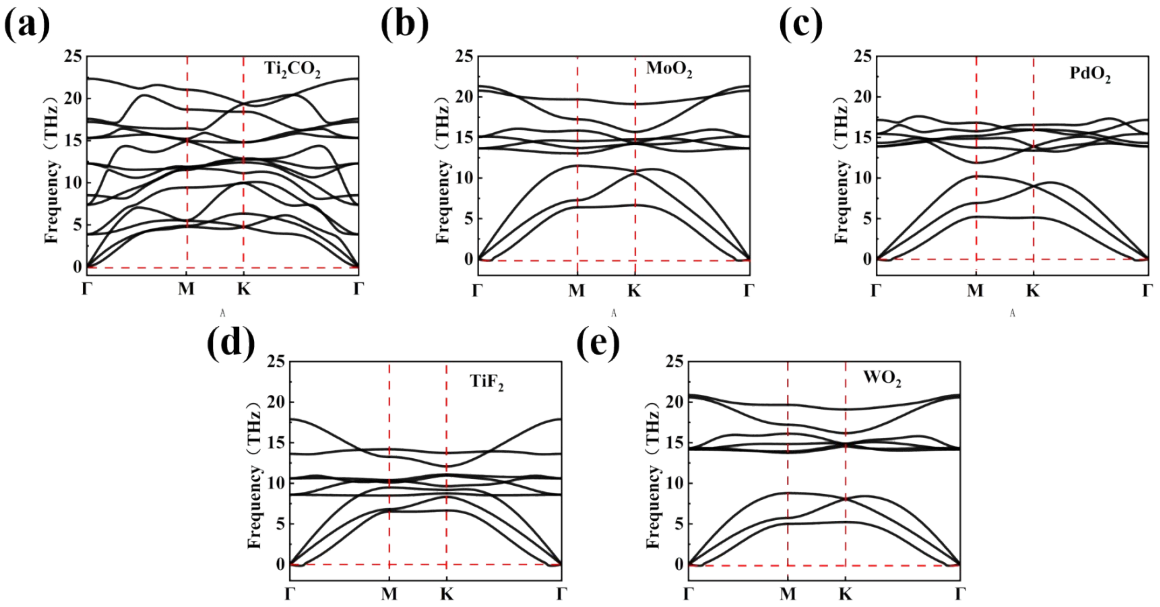

Fig. S3. The phonon spectra for (a) Ti_2CO_2, (b) MoO_2, (c) PdO_2, (d) TiF_2 and (e) WO_2 monolayers.

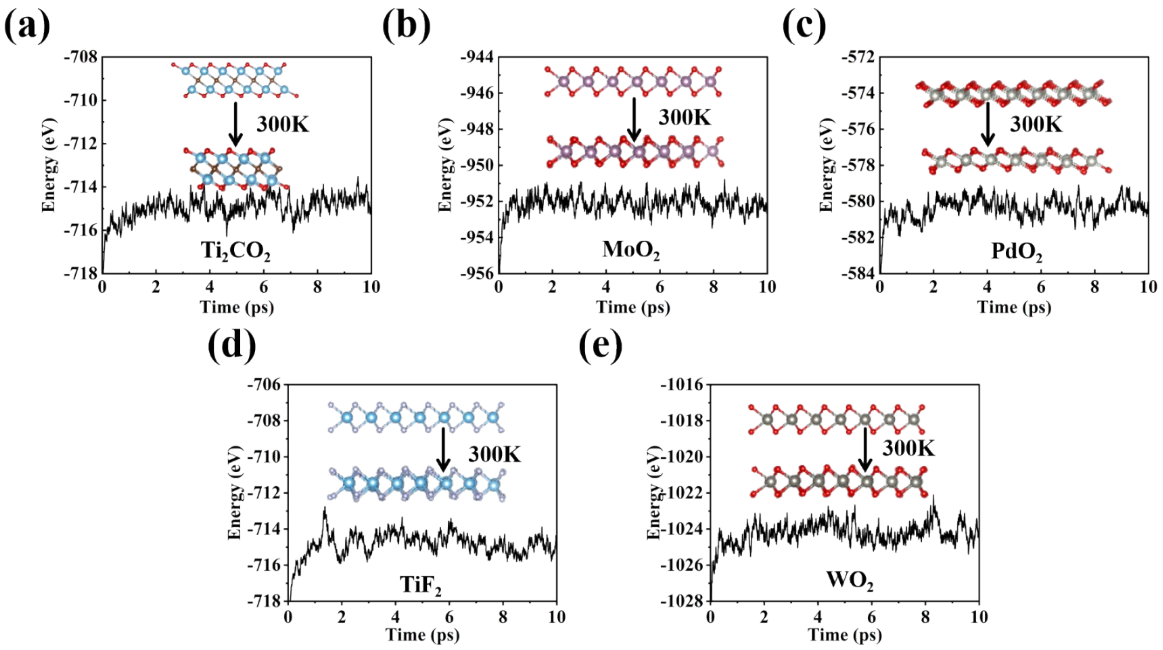

Fig. S4. The total energy evolution curves for (a) Ti_2CO_2, (b) MoO_2, (c) PdO_2, (d) TiF_2 and (e) WO_2 monolayers from the AIMD simulation.

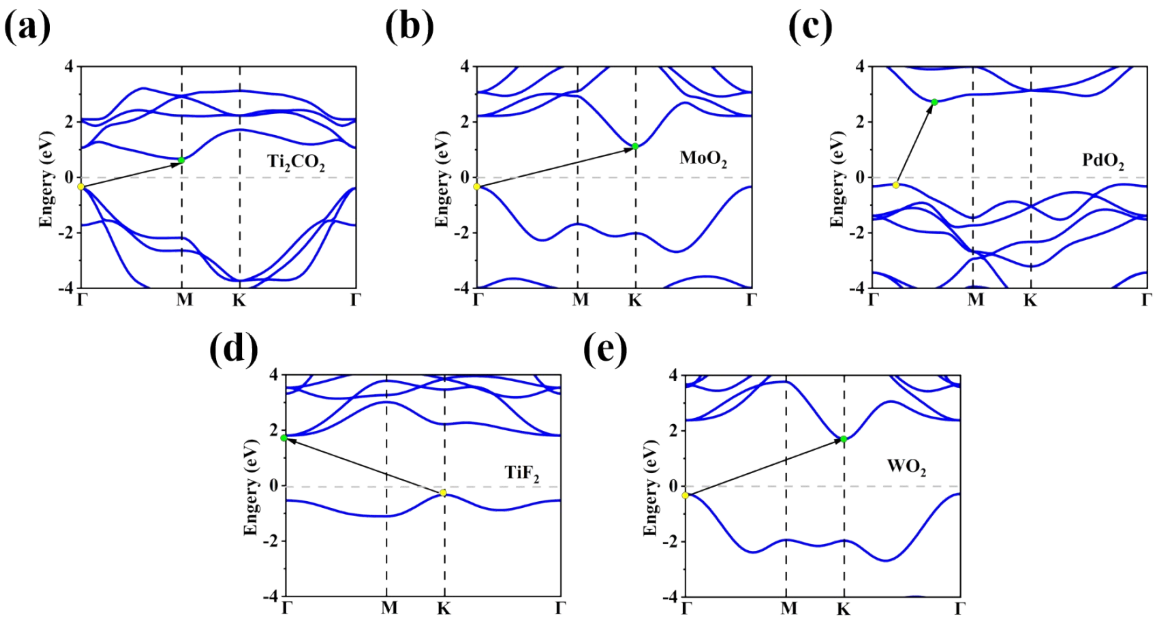

Fig. S5. The band structures for (a) Ti_2CO_2, (b) MoO_2, (c) PdO_2, (d) TiF_2 and (e) WO_2 monolayers at the HSE06 levels.

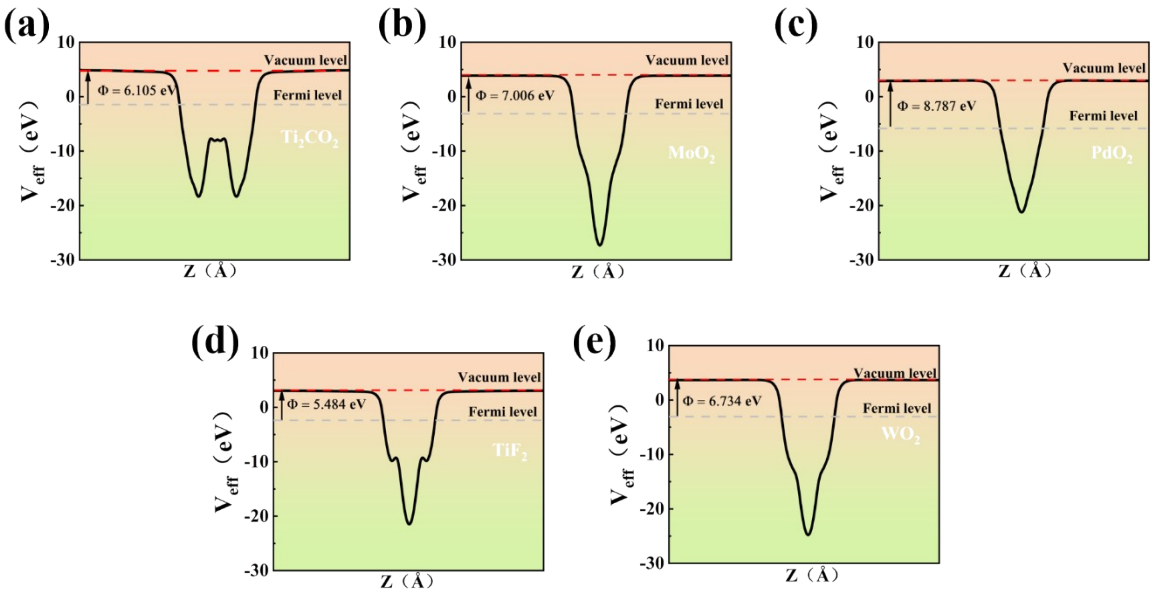

Fig. S6. The planar-averaged electrostatic potential along the z-axis for (a) Ti_2CO_2, (b) MoO_2, (c) PdO_2, (d) TiF_2 and (e) WO_2 monolayers.

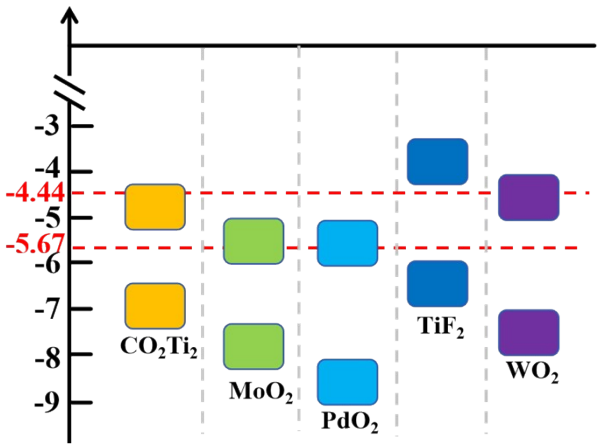

Fig. S7. The band edges position for different monolayers.

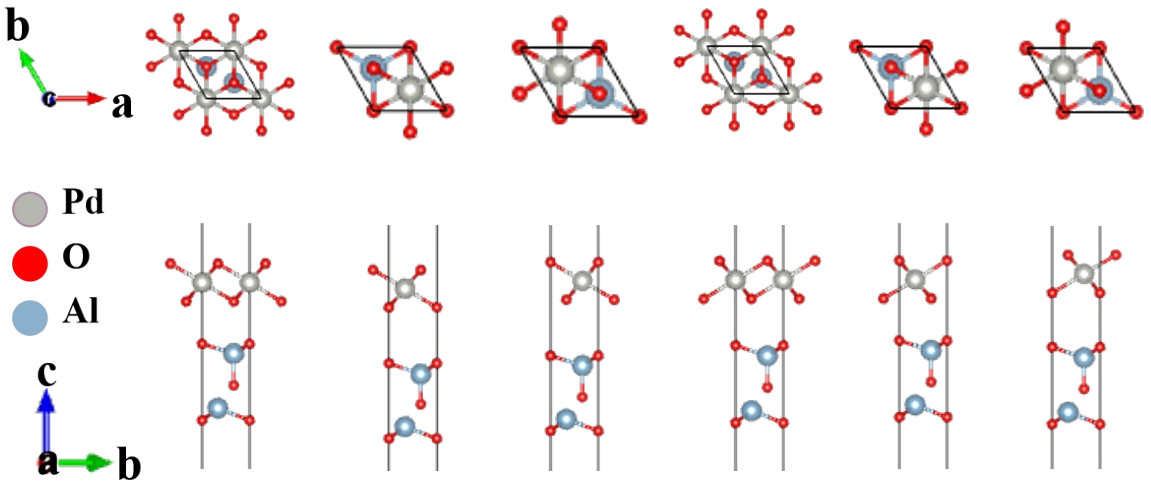

Fig. S8. Different stacking configurations of polarized-up and nonpolar materials.

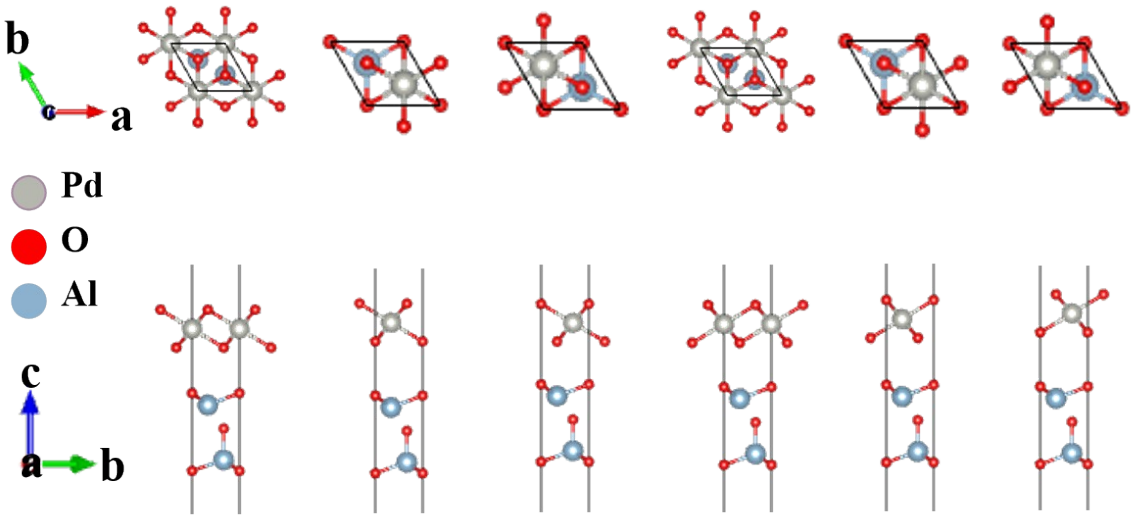

Fig. S9. Different stacking configurations of polarized-down and nonpolar materials.

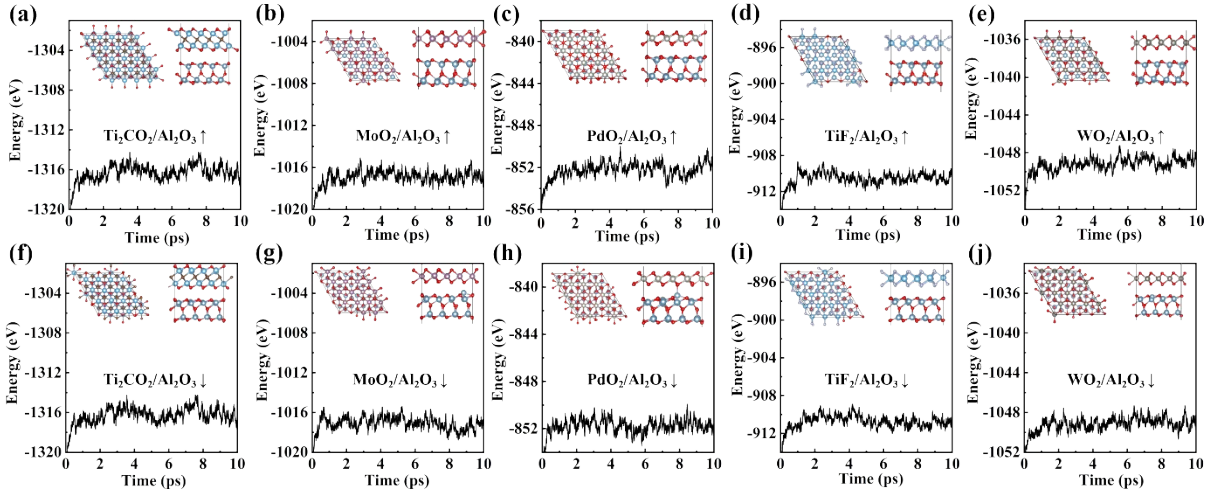

Fig. S10. The evolution of total energy for (a) Ti_2CO_2/Al_2O_3-P↑, (b) MoO_2/Al_2O_3-P↑, (c) PdO_2/Al_2O_3-P↑, (d) TiF_2/Al_2O_3-P↑, (e) WO_2/Al_2O_3-P↑, (f) Ti_2CO_2/Al_2O_3-P↓, (g) MoO_2/Al_2O_3-P↓, (h) PdO_2/Al_2O_3-P↓, (i) TiF_2/Al_2O_3-P↓and (j) WO_2/Al_2O_3-P↓ heterostructures.

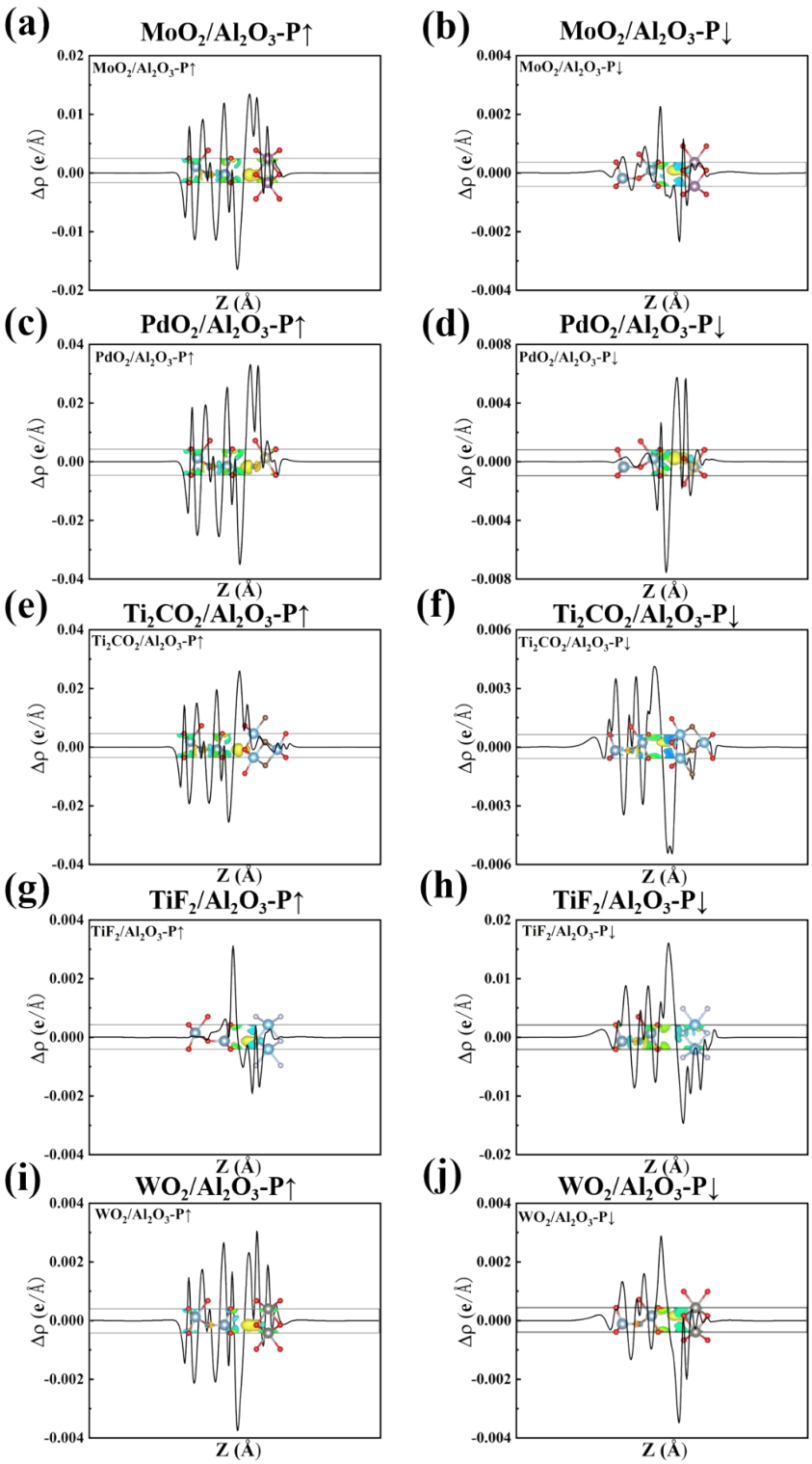

Fig. S11. The charge density difference of (a) MoO_2/Al_2O_3-P↑, (b) PdO_2/Al_2O_3-P↑, (c) Ti_2CO_2/Al_2O_3-P↑, (d) TiF_2/Al_2O_3-P↑, (e) WO_2/Al_2O_3-P↑, (f) MoO_2/Al_2O_3-P↓, (g) PdO_2/Al_2O_3-P↓, (h) Ti_2CO_2/Al_2O_3-P↓, (i) TiF_2/Al_2O_3-P↓and (e) WO_2/Al_2O_3-P↓ heterostructures.

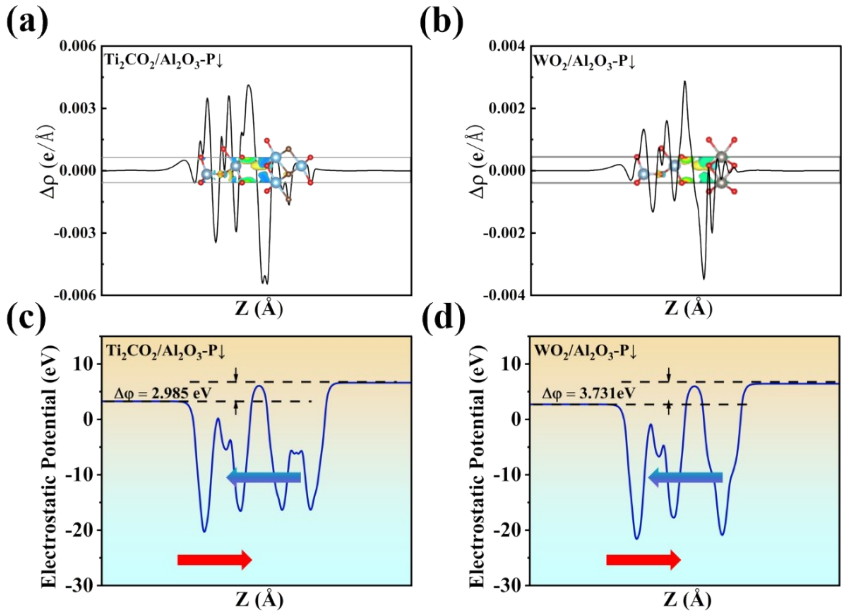

Fig. S12. The charge density difference of (a) Ti_2CO_2/Al_2O_3-P↓, and (b) WO_2/Al_2O_3-P↓， the planar-averaged electrostatic potential along the z-axis of (c) Ti_2CO_2/Al_2O_3-P↓, and (d)WO_2/Al_2O_3-P↓.(Red arrows represent the electric field direction of Al_2O_3, while blue arrows represent the electric field direction of the heterostructure).

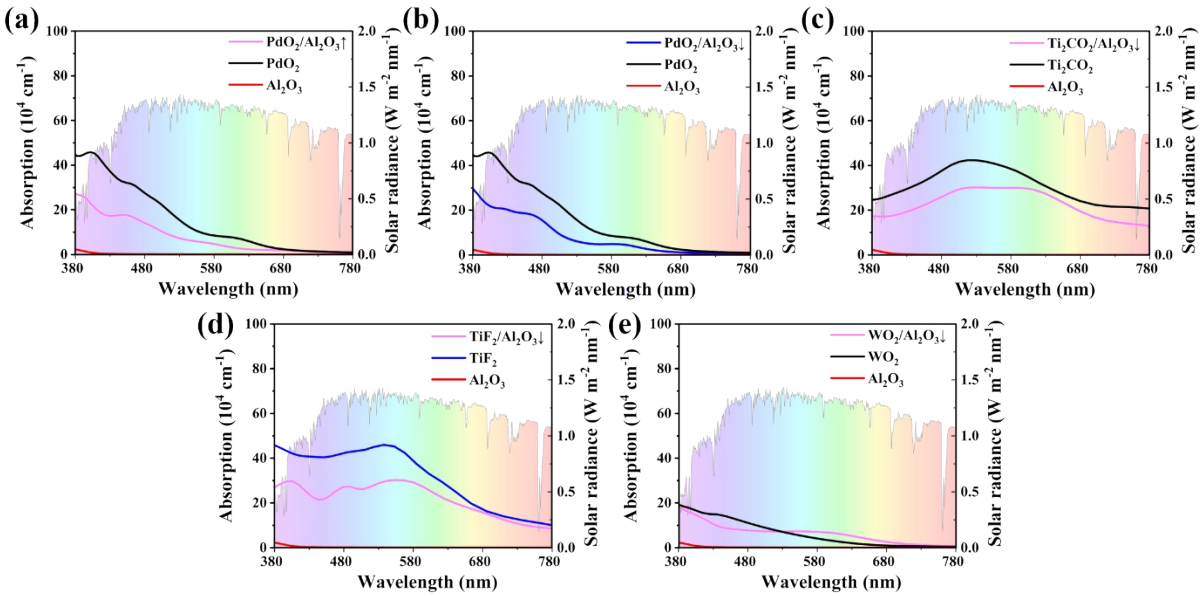

Fig. S13. The calculated optical absorption coefficients for (a) PdO_2/Al_2O_3-P↓ , (b) PdO_2/Al_2O_3-P↓ , (c) Ti_2CO_2/Al_2O_3-P↓ , (d) TiF_2/Al_2O_3-P↓ and (e) WO_2/Al_2O_3-P↓ heterostructures.

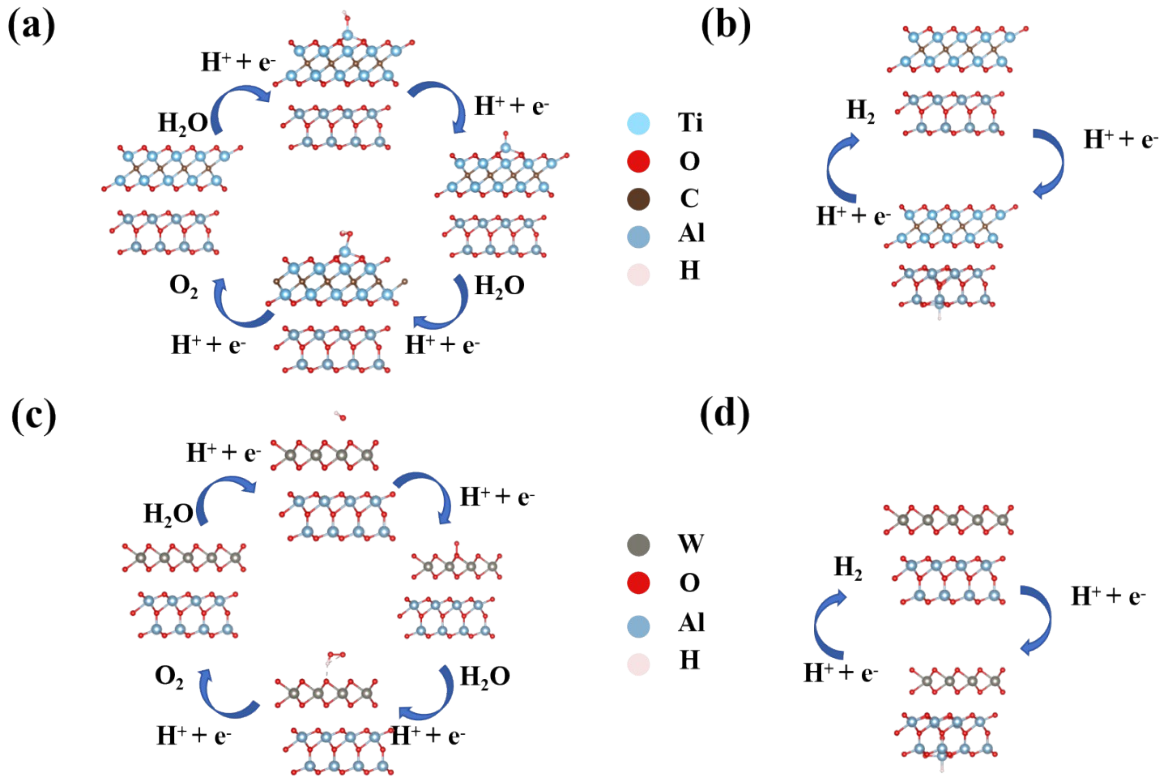

Fig. S14. Optimized structures showing the adsorption configurations of (a) Ti_2CO_2/Al_2O_3-P↓ and (b) WO_2/Al_2O_3-P↓ heterostructure on the surface.

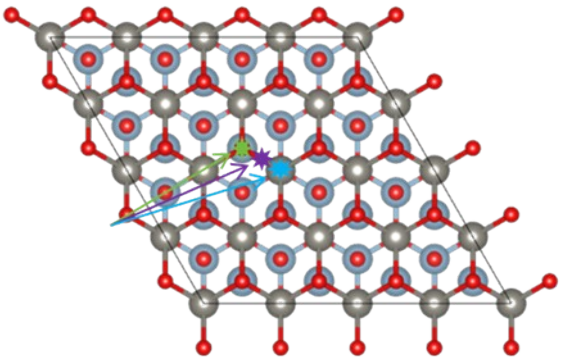

Fig. S15. The different colors in the schematic diagram of adsorption site selection indicate: (a) green for the top site, (b) purple for the bridge site, and (c) blue for the hollow site.

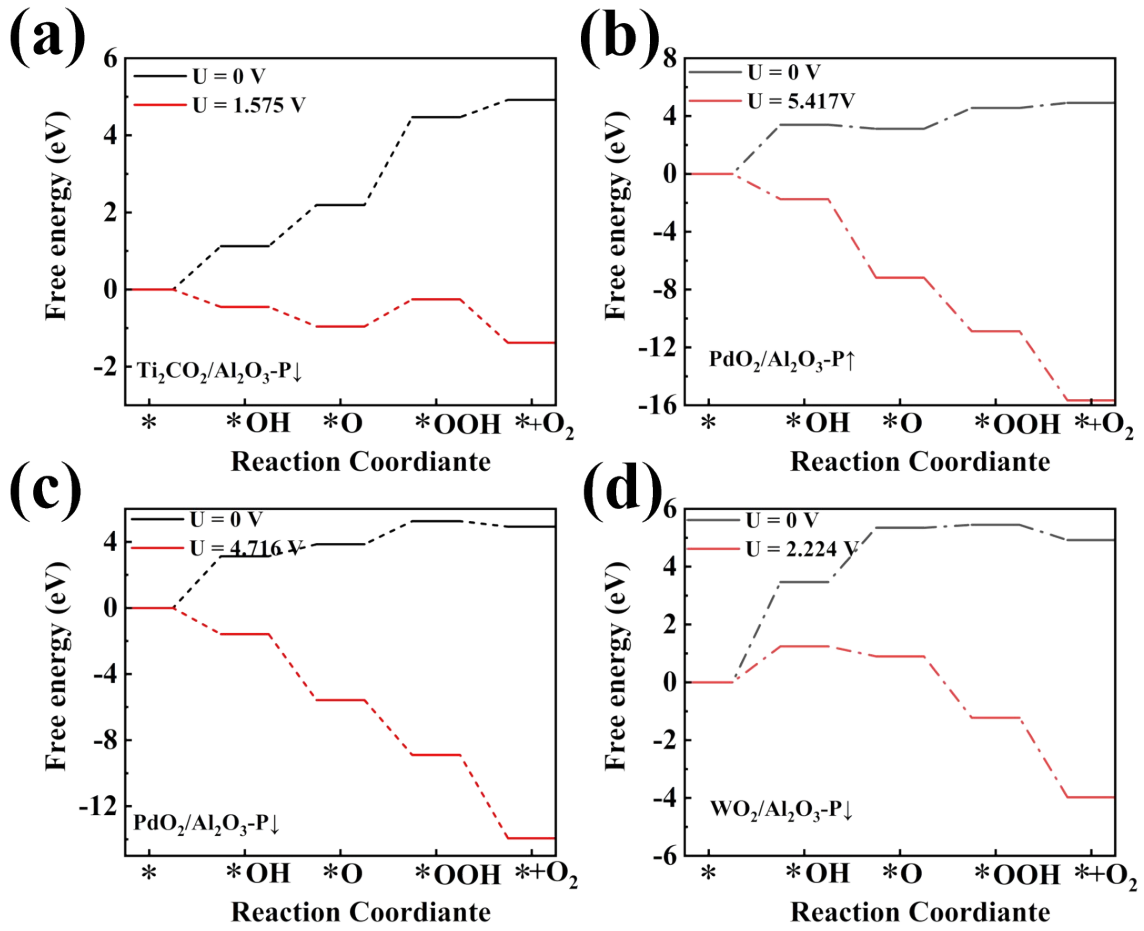

Fig. S16. The calculated Gibbs free energy difference ΔG for (a) Ti_2CO_2/Al_2O_3-P↓, (b) PdO_2/Al_2O_3-P↑, (c) PdO_2/Al_2O_3-P↓ and (d) WO_2/Al_2O_3-P↓ heterostructures.

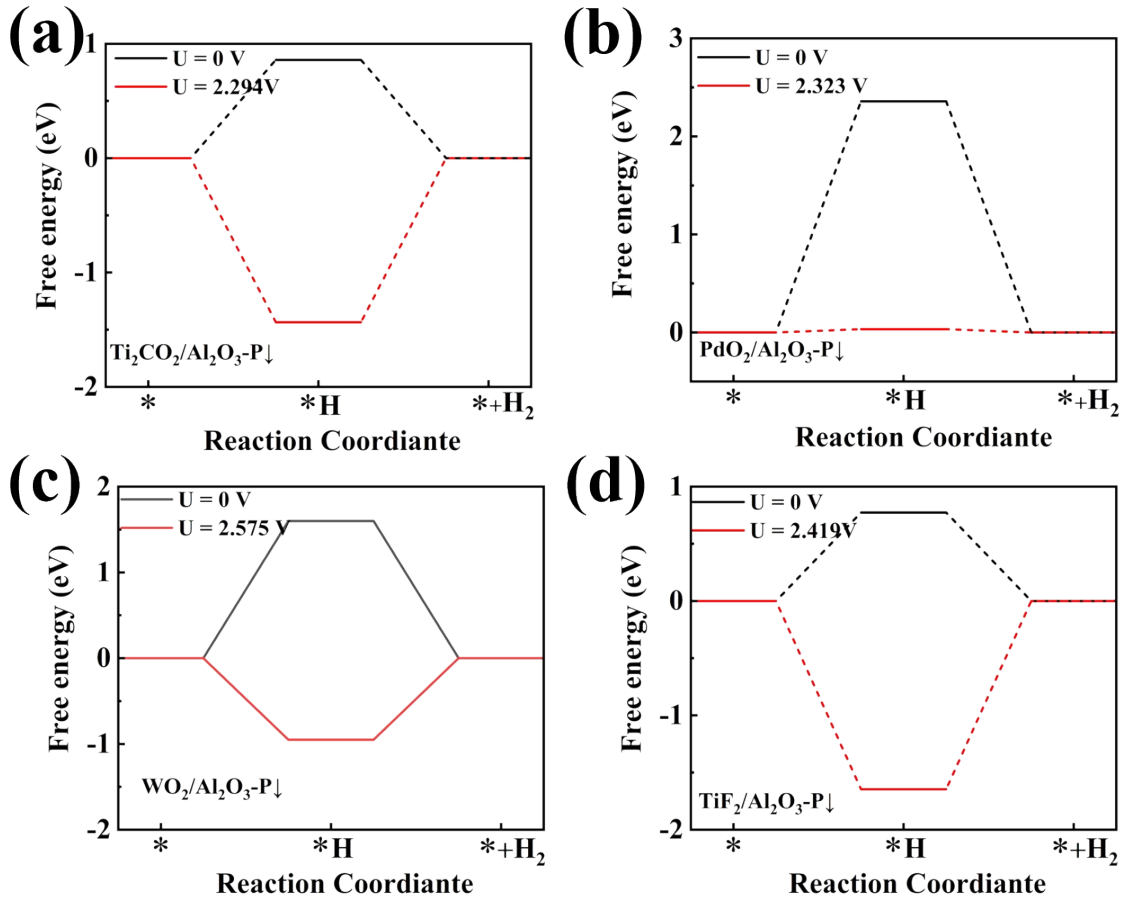

Fig. S17. The calculated Gibbs free energy difference ΔG for (a) Ti_2CO_2/Al_2O_3-P↓, (b) PdO_2/Al_2O_3-P↓, (c) WO_2/Al_2O_3-P↓ and (d) TiF_2/Al_2O_3-P↓ heterostructures.